Quantum backflow current in a ring: Optimal bounds and fractality

Arseni Goussev [1,2], Felix Quinque [3], Jaewoo Joo,[3] and Andrew Burbanks [3]
[1]*Section of Mathematics, University of Geneva, Rue du Conseil-Général 7-9, 1205 Genève, Switzerland*
[2]*Quantum Physics Corner Ltd, 20-22 Wenlock Road, London N1 7GU, United Kingdom*
[3]*School of Mathematics and Physics, University of Portsmouth, Portsmouth PO1 3HF, United Kingdom*

(Received 27 March 2024; accepted 18 July 2024; published 12 August 2024)

The probability density of a quantum particle moving freely within a circular ring can exhibit local flow patterns inconsistent with its angular momentum, a phenomenon known as quantum backflow. In this study, we examine a quantum particle confined to a ring and prepared in a state composed of a fixed (yet arbitrary) number of lowest-energy eigenstates with nonnegative angular momentum. We investigate the time-dependent behavior of the probability current at a specified point along the ring's circumference. We establish precise lower and upper bounds for this probability current, thereby delineating the exact scope of the quantum backflow effect. We also present an analytical expression for a quantum state that yields a record-high backflow probability transfer, reaching over 95% of the theoretical bound. Furthermore, our investigation yields compelling numerical and analytical evidence supporting the conjecture that the current-versus-time function associated with states maximizing backflow probability transfer forms a fractal curve with a dimension of 7/4. The observed fractality may provide a characteristic, experimentally relevant signature of quantum backflow near the probability-transfer bound.

DOI: 10.1103/PhysRevA.110.022216

I. INTRODUCTION

In classical mechanics, a particle always moves in the direction of its momentum, which serves as a measure of the intensity of the particle's motion. In quantum mechanics, however, the situation can be strikingly different: the probability density of a quantum particle may in fact flow against its momentum. This intriguing phenomenon, initially recognized within the context of the arrival time problem [1–3], is known as quantum backflow (QB).

The first systematic examination of QB was conducted by Bracken and Melloy [4]. They examined the time evolution of the probability density of a free particle on a line constrained to move with positive momentum and addressed the (classically impossible) flow of the probability density in the negative direction. Their most notable finding was the fact that the total probability transported through a fixed spatial point cannot exceed a certain threshold, commonly known as the Bracken-Melloy (BM) bound. The BM bound is independent of the particle's mass, the observation time interval, or the Planck constant. Numerical estimates indicate the BM bound to approximately equal 0.0384517 [5,6]. While the exact value of the BM bound remains unknown, it has been recently proven to lie between 0.0315 and 0.0725 [7].

The phenomenon of QB has been addressed in the literature across various scenarios and formulations. Among the problems explored are QB against a constant force [8], the spatial extent of the backflow proability current [5,9,10], the relationship between QB and the arrival time problem [11–14], QB for rotational motion [15–18], QB in many-particle systems [19,20] and in the presence of noisy and dissipative environments [21–23], backflow in relativistic systems [24–28], QB across a black hole horizon [29], and the classical limit of QB [30–33]. Multiple analytical examples of states exhibiting probability backflow have been constructed [4,5,30,34,35]. QB has been explored both in phase space [4,21,36,37] and as variations of the quantum reentry problem [38–41]. The reader is directed to Ref. [42] for an elementary introduction to the phenomenon of QB and to Refs. [43–45] for non-technical discussions of its physical interpretation and nonclassical character.

So far, direct experimental observation of QB remains elusive, despite existing proposals exploring methods to detect the effect using Bose-Einstein condensates [46,47]. The challenges associated with the experimental realization of QB for a particle on a line stem from two main factors. First, only a minute portion of the overall probability, given by the BM bound, can theoretically be transported in the "wrong" direction. Second, the quantum states that exhibit backflow probability transfer near the BM bound are characterized by their infinite spatial extent and infinite energy [30], rendering them challenging to produce in a laboratory environment. However, although the first experimental demonstration of QB is still forthcoming, the effect has already been successfully simulated in classical optics experiments [48–50] and on a genuine quantum computer [51].

A promising avenue for future experimental realization of QB involves a quantum particle rotating freely in a circular ring [17]. In this scenario, the particle is prepared in a superposition of energy and angular momentum eigenstates with nonnegative angular momentum, and the observed quantity is the probability current through a fixed point on the ring. Contrary to classical mechanical predictions, the quantum mechanical probability current can assume negative values, thereby manifesting the phenomenon of QB. For this scenario, it has been demonstrated [17] that the total backflow

probability transfer over a finite time interval can exceed the BM bound by more than threefold, reaching approximately 0.116816. Moreover, the particle-in-a-ring states exhibiting significant backflow probability transfer have been shown to possess finite energy (and, due to the nature of the problem, finite spatial extent), rendering them more suitable for experimental realization.

In this paper, we explore the QB phenomenon for a particle confined to a circular ring, scrutinizing the probability current at a fixed point along the ring's circumference. Our study yields two primary findings. First, we establish optimal lower and upper bounds on the probability current for the most general state of the system, encompassing a fixed (yet arbitrary) number of lowest-energy eigenstates with nonnegative momentum. In other words, we determine the minimally and maximally attainable values of the probability current associated with the most general superposition of nonnegative angular momentum states, all with energies not exceeding a specified (yet arbitrary) threshold. Second, we propose a conjecture regarding the time dependence of the probability current of the state maximizing backflow probability transfer, or states characterized by backflow probability transfers nearing the theoretical limit. More specifically, we conjecture that this probability current is a fractal function of time, with a fractal dimension of 7/4, and present compelling numerical and analytical evidence in support of our conjecture. We suggest the possibility that fractal characteristics may provide an experimental signature of QB near the probability-transfer bound, important for future investigations.

The paper is organized as follows. In Sec. II, we define the system and introduce the dimensionless probability current, which will serve as the central object of study throughout the rest of the paper. In Sec. III, we derive the optimal bounds for the probability current. Section IV is dedicated to summarizing crucial facts about backflow probability transfer, laying the groundwork for the subsequent discussion. Section V explores the time dependence of the probability current associated with the backflow-maximizing state and presents the numerical calculation of its fractal dimension. In Sec. VI, we construct an accurate analytical approximation for the backflow-maximizing state and determine that the fractal dimension of its corresponding current-versus-time function is 7/4, in good agreement with the numerical value obtained in Sec. V. (In brief, Secs. II and IV primarily introduce the system and review relevant existing results, whereas Secs. III, V, and VI present original findings.) We summarize our findings and provide closing remarks in Sec. VII.

II. PROBABILITY CURRENT

We consider a particle of mass M freely moving on a circular ring of radius R. The wave function of the particle is denoted by $\psi(\theta, T)$ and satisfies the Schrödinger equation

$$i\hbar\frac{\partial\psi}{\partial T} = -\frac{\hbar^2}{2MR^2}\frac{\partial^2\psi}{\partial\theta^2}. \tag{1}$$

Here, θ is the angle coordinate of the particle, and T is time. The wave function is subject to periodic boundary conditions, $\psi(-\pi, T) = \psi(\pi, T)$. The general solution to Eq. (1) has the form of a linear combination of energy eigenstates

$$\phi_m(\theta, T) = \frac{1}{\sqrt{2\pi}}e^{im\theta - iE_mT/\hbar},$$

each labeled by an integer $m \in \mathbb{Z}$ and characterized by the energy value

$$E_m = \frac{\hbar^2 m^2}{2MR^2}.$$

Since $(-i\hbar\partial/\partial\theta)\phi_m = (m\hbar)\phi_m$, the eigenstates ϕ_m are also characterized by definite values of angular momentum $m\hbar$.

In what follows, we only consider quantum wave packets with nonnegative angular momentum. Thus, let ψ_N be a wave packet comprised of eigenstates ϕ_m with $0 \leqslant m \leqslant N$, namely,

$$\psi_N(\theta, T) = \frac{1}{\sqrt{2\pi}}\sum_{m=0}^{N} c_m e^{im\theta - iE_mT/\hbar}. \tag{2}$$

The wave packet is assumed to be normalized to unity, $\int_{-\pi}^{\pi} d\theta\, |\psi_N(\theta, T)|^2 = 1$, implying that the expansion coefficients satisfy

$$\sum_{m=0}^{N} |c_m|^2 = 1. \tag{3}$$

By construction, any angular momentum measurement conducted on ψ_N is certain to yield a nonnegative result.

The main focus of present study is the probability current J_N through an arbitrarily fixed point on the ring, taken to be $\theta = 0$ for concreteness

$$J_N(T) = \frac{\hbar}{MR^2}\,\mathrm{Im}\left\{\psi_N^*(\theta, T)\frac{\partial\psi_N(\theta, T)}{\partial\theta}\right\}\Bigg|_{\theta=0}. \tag{4}$$

QB occurs when the probability current is negative, i.e., when $J_N(T) < 0$ for some T.

It is convenient to introduce dimensionless time t and dimensionless probability current j_N as

$$T = \frac{2MR^2}{\hbar}t, \quad J_N(T) = \left(\frac{2MR^2}{\hbar}\right)^{-1} j_N(t). \tag{5}$$

Substituting Eq. (2) into Eq. (4), and taking into account transformations (5), we obtain the following expression for the dimensionless probability current:

$$j_N(t) = \frac{1}{2\pi}\sum_{m,n=0}^{N} c_m^* c_n (m+n) e^{i(m^2-n^2)t}. \tag{6}$$

III. OPTIMAL BOUNDS ON THE PROBABILITY CURRENT

How small and how large can the probability current possibly be? In this section we answer this question by showing that

$$\frac{N(N+1)}{4\pi}\left(1 - \sqrt{\frac{4N+2}{3N}}\right) \leqslant j_N(t) \leqslant \frac{N(N+1)}{4\pi}\left(1 + \sqrt{\frac{4N+2}{3N}}\right), \tag{7}$$

for all t, and by finding the expansion coefficients $\{c_m\}_{m=0}^N$ of the states corresponding to the extreme values of the current.

We begin by rewriting Eq. (6) as an expectation value

$$j_N(t) = \langle\psi_N(t)|\hat{j}_N|\psi_N(t)\rangle. \tag{8}$$

Here,

$$|\psi_N(t)\rangle = \sum_{m=0}^{N} c_m e^{-im^2 t}|m\rangle \tag{9}$$

is the particle's state, $|0\rangle, |1\rangle, \ldots, |N\rangle$ are angular momentum eigenstates satisfying the orthonormality condition $\langle m|n\rangle = \delta_{mn}$, and

$$\hat{j}_N = \frac{1}{2\pi}\sum_{m,n=0}^{N} |m\rangle(m+n)\langle n| \tag{10}$$

is the operator representing the probability current on the subspace of the Hilbert space spanned by $\{|m\rangle\}_{m=0}^N$. The state ψ_N is assumed to be normalized, i.e., $\langle\psi_N|\psi_N\rangle = 1$, which is equivalent to Eq. (3).

We now look for eignevectors $|\chi\rangle$ of $\hat{j}_N$ that are of the form

$$|\chi\rangle = A\sum_{m=0}^{N}(m+a)|m\rangle, \tag{11}$$

where a and A are some (yet to be determined) constants. Substituting Eqs. (10) and (11) into the eigenequation

$$\hat{j}_N|\chi\rangle = \lambda|\chi\rangle,$$

we obtain

$$\frac{1}{2\pi}\sum_{m,n=0}^{N}(m+n)(n+a)|m\rangle = \lambda\sum_{m=0}^{N}(m+a)|m\rangle.$$

Then, using the identities $\sum_{n=0}^N n = \frac{1}{2}N(N+1)$ and $\sum_{n=0}^N n^2 = \frac{1}{6}N(N+1)(2N+1)$, we evaluate the sum over n in the last equation to get

$$\frac{(N+1)(N+2a)}{4\pi}\sum_{m=0}^{N}\left(m + \frac{N(2N+1+3a)}{3(N+2a)}\right)|m\rangle = \lambda\sum_{m=0}^{N}(m+a)|m\rangle.$$

The last equation is satisfied if and only if

$$a = \frac{N(2N+1+3a)}{3(N+2a)} \tag{12}$$

and

$$\lambda = \frac{(N+1)(N+2a)}{4\pi}. \tag{13}$$

Equation (12) is quadratic in a and has two roots, a_+ and a_-, given by

$$a_\pm = \pm\sqrt{\frac{N(2N+1)}{6}}. \tag{14}$$

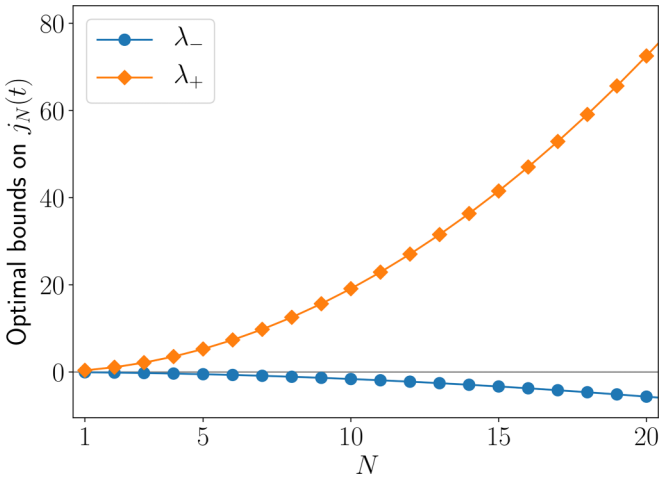

FIG. 1. Eigenvalues λ_+ and λ_- as functions of N, given by Eq. (15). The gray horizontal line shows the level of zero probability current.

Then, according to Eq. (13), the corresponding eigenvalues, λ_+ and λ_-, read

$$\lambda_\pm = \frac{N(N+1)}{4\pi}\left(1 \pm \sqrt{\frac{4N+2}{3N}}\right). \tag{15}$$

Clearly, $\lambda_+ > 0$ and $\lambda_- < 0$, for all $N \geqslant 1$. Figure 1 illustrates the dependence of the eigenvalues on N. Finally, eigenvectors $|\chi_+\rangle$ and $|\chi_-\rangle$ corresponding to the eigenvalues λ_+ and λ_- are found by substituting Eq. (14) into Eq. (11):

$$|\chi_\pm\rangle = A_\pm\sum_{m=0}^{N}\left(m \pm \sqrt{\frac{N(2N+1)}{6}}\right)|m\rangle. \tag{16}$$

It is straightforward to verify (see Appendix A) that the normalization constants, A_+ and A_- are given by

$$A_\pm = \left[N(N+1)\left(\frac{2N+1}{3} \pm \sqrt{\frac{N(2N+1)}{6}}\right)\right]^{-1/2}. \tag{17}$$

We now make the observation that λ_+ and λ_-, given by Eq. (15), are the only nonzero eigenvalues of the operator $\hat{j}_N$. Indeed, as shown in Appendix B, $\hat{j}_N$ admits the following decomposition:

$$\hat{j}_N = \lambda_+|\chi_+\rangle\langle\chi_+| + \lambda_-|\chi_-\rangle\langle\chi_-|. \tag{18}$$

Then, using Eq. (8), we get

$$j_N(t) = \lambda_+|\langle\chi_+|\psi_N(t)\rangle|^2 + \lambda_-|\langle\chi_-|\psi_N(t)\rangle|^2. \tag{19}$$

Since $\lambda_+ > 0$, $\lambda_- < 0$, and $0 \leqslant |\langle\chi_\pm|\psi_N(t)\rangle| \leqslant 1$, we conclude that

$$\lambda_- \leqslant j_N(t) \leqslant \lambda_+,$$

which is equivalent to Eq. (7). The probability current $j_N(t)$ reaches its extreme values, λ_+ and λ_-, when $|\psi_N(t)\rangle$ coincides (up to a global phase factor) with the states $|\chi_+\rangle$ and $|\chi_-\rangle$, respectively.

IV. PROBABILITY TRANSFER

We now consider the amount of probability P_N passing through the point $\theta = 0$ over a time interval Δ. More precisely,

$$P_N = \int_{-\Delta/2}^{\Delta/2} dT\, J_N(T),$$

where J_N is the probability current defined by Eq. (4). In terms of the dimensionless current, defined in Eq. (5), the probability transfer P_N reads

$$P_N = \int_{-\alpha}^{\alpha} dt\, j_N(t), \tag{20}$$

where

$$\alpha = \frac{\hbar\Delta}{4MR^2}$$

is a dimensionless parameter.

As demonstrated in Ref. [17], P_N can be negative and has a finite greatest lower bound. In the following section of this paper, we explore the probability current $j_N(t)$ generated by a quantum state characterized by the value of P_N that is very close to the greatest lower bound. To set the stage for this exploration, we now briefly summarize some findings of Ref. [17] that are particularly relevant to the ensuing discussion.

The substitution of Eq. (6) into Eq. (20), followed by evaluation of the integral over t, yields

$$P_N = \frac{\alpha}{\pi}\sum_{m=0}^{N}\sum_{n=0}^{N} c_m^* c_n (m+n)\,\mathrm{sinc}[\alpha(m^2-n^2)], \tag{21}$$

where $\mathrm{sinc}\, z = (\sin z)/z$. To determine the (negative) optimal lower bound for probability transfer, one needs to minimize P_N within the $(N+1)$-dimensional space of vectors $(c_0, c_1, \ldots, c_N)$, while adhering to the normalization constraint (3). This is accomplished through the method of Lagrange multipliers, whereby one conducts unconstrained minimization of the function

$$\mathcal{L}(c_0, c_1, \ldots, c_N) = P_N - \mu\sum_{m=0}^{N} c_m^* c_m,$$

where μ is a Lagrange multiplier. In view of Eq. (21), the Euler-Lagrange equation corresponding to this minimization problem reads

$$\frac{\alpha}{\pi}\sum_{n=0}^{N}(m+n)\,\mathrm{sinc}[\alpha(m^2-n^2)]c_n = \mu c_m.$$

This equation defines an eigenproblem, in which μ plays the role of the eigenvalue corresponding to the eigenvector $(c_0, c_1, \ldots, c_N)$. The eigenproblem is then solved numerically, resulting in a spectrum of $(N+1)$ (not necessarily distinct) eigenvalues, $\mu_0, \mu_1, \ldots, \mu_N$. The smallest eigenvalue corresponds to the desired minimal probability transfer

$$P_N^{\min} \equiv \min P_N = \min\{\mu_0, \mu_1, \ldots, \mu_N\}.$$

It is important to keep in mind that $P_N^{\min}$ depends on the system parameter α.

The function $P_N^{\min}$ was numerically computed in Ref. [17]. In particular, the study demonstrated that

$$\inf_{\alpha}\lim_{N\to\infty} P_N^{\min} \simeq -0.116816, \tag{22}$$

thus providing the greatest lower bound on the probability transfer associated with the most general superposition of particle-in-a-ring states with nonnegative angular momentum. The bound presented in Eq. (22) is achieved for the system parameter value close to

$$\alpha = 1.163635. \tag{23}$$

We conclude this section by noting that the probability transfer, P_N, can be represented as the sum of two terms, one nonnegative and the other nonpositive

$$P_N = P_N^{(+)} + P_N^{(-)}, \tag{24}$$

where

$$P_N^{(\pm)} = \frac{1}{4\pi a_\pm}\int_{-\alpha}^{\alpha} dt \left|\sum_{m=0}^{N} c_m (m+a_\pm) e^{-im^2 t}\right|^2. \tag{25}$$

The fact that $a_+ = -a_- > 0$ [see Eq. (14)] implies that

$$P_N^{(+)} \geqslant 0 \quad \text{and} \quad P_N^{(-)} \leqslant 0.$$

Appendix C provides a derivation of this representation and elucidates its relationship with Eq. (21). Currently, the practical significance of this representation remains unclear. However, the noteworthy aspect that $P_N^{(+)} \geqslant 0$ and $P_N^{(-)} \leqslant 0$ is nontrivial, and it may prove valuable in future studies, especially when attempting to establish precise bounds for probability transfer.

V. FRACTAL DIMENSION OF THE BACKFLOW-MAXIMIZING CURRENT

We now explore a specific particle-in-a-ring state with nonnegative angular momentum, characterized by a value of probability transfer very close to the estimated bound given in Eq. (22). The state was obtained via numerical minimization of the probability transfer (21), with $N = 9999$ and α given by Eq. (23), subject to the normalization constraint, Eq. (3). Employing somewhat loose terminology, we will refer to this state as a "backflow-maximizing" state.

More precisely, the backflow-maximizing state $|\psi_{\mathrm{bm}}(t)\rangle$ considered here is defined as $|\psi_{9999}(t)\rangle$ [see Eq. (9)] with

$$\begin{aligned} c_0 &= 9.443114018508278473 \times 10^{-1},\\ c_1 &= -3.152130460659169908 \times 10^{-1},\\ c_2 &= 7.894329104096091398 \times 10^{-2},\\ &\cdots\cdots\cdots\cdots\cdots\cdots\cdots\cdots\\ c_{9999} &= 6.151844737832881660 \times 10^{-10}. \end{aligned} \tag{26}$$

The complete list of expansion coefficients is provided in the Supplemental Material [52]. The numerically computed value of the probability transfer, corresponding to $|\psi_{\mathrm{bm}}\rangle$, equals -0.11681564958330892. Hereinafter, our analysis maintains a fixed value for α as specified by Eq. (23).

As noted in Ref. [17], the backflow-maximizing state $|\psi_{\mathrm{bm}}\rangle$ is characterized by a finite mean energy, which stands in stark

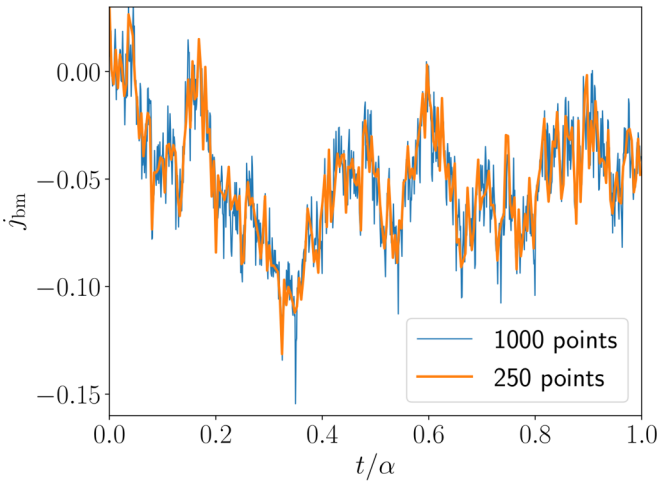

FIG. 2. Probability current for the backflow-maximizing state. The two graphs was obtained by computing $j_{9999}(t)$ from Eq. (6), with c_m's given by Eq. (26), at two different sets of instances between $t = 0$ and $t = \alpha$. One thousand equally spaced points were used to produce the thin (blue) curve, whereas 250 equally spaced points were used for the thick (orange) curve. The value of α is given by Eq. (23).

contrast to the infinite mean energy observed in the linear case. In the units used in the present paper, the mean energy of $|\psi_{\rm bm}\rangle$ is given by

$$\langle E\rangle = \frac{\hbar^2}{2MR^2}\sum_{m=0}^{9999} m^2 c_m^2 \simeq 0.082837 \times \frac{\hbar^2}{MR^2}.$$

Figure 2 shows the graph of the probability current $j_{\rm bm}(t)$, computed numerically for two different sets of points between $t = 0$ and $t = \alpha$, using Eq. (6), for the backflow-maximizing state, $|\psi_{\rm bm}(t)\rangle$. In other words, $j_{\rm bm}(t)$ is $j_{9999}(t)$ [see Eq. (6)] with c_m's given by Eq. (26). The graph appears to be highly irregular. (In fact, as we will argue below, it represents a fractal curve.) The visual appearance of the graph strongly depends on the particular choice of instances used to evaluate the function $j_{\rm bm}(t)$ and plot the graph. The thin (blue) curve in Fig. 2 was obtain by computing $j_{\rm bm}$ at 1000 equally spaced instances between $t = 0$ and $t = \alpha$, whereas 250 equally spaced points were used to plot the thick (orange) curve.

The probability current for the backflow-maximizing state of a particle in a ring (see Fig. 2) is significantly distinct from the corresponding probability current in the particle-on-a-line scenario (see, e.g., Fig. 6 in Ref. [6]). In the later case, the current is consistently negative within the observed time window for probability transfer, and is represented by a smooth curve. In contrast, the previous case displays sign changes and exhibits a markedly irregular, fractal-like graph. Exploring this difference is both interesting and important, especially given the proposed direct measurement of current as a strategy for the first experimental observation of quantum backflow [4]. To this end, we quantitatively examine the fuzziness and irregularity of the current-versus-time curve for the ring geometry by evaluating its fractal dimension. The remainder of this section focuses on the numerical computation of the fractal dimension, while Sec. VI provides analytical arguments supporting the numerical results.

Let us now evaluate the Higuchi dimension [53], denoted by $D_{\rm H}$, of the function $j_{\rm bm}(t)$ on the interval $0 < t < \alpha$ (see Fig. 2). The Higuchi dimension is widely used as an estimator of the box-counting dimension for bounded functions. (See Ref. [54] for the analysis of the robustness and limitations of this method.)

Our calculation of the Higuchi dimension of $j_{\rm bm}(t)$ follows the procedure presented in Ref. [53]. We compute the function $j_{\rm bm}(t)$ at $S = 262\,144 = 2^{18}$ equally spaced time points between 0 and α, thus obtaining the sequence

$$\mathcal{J} = \{\mathcal{J}(1), \mathcal{J}(2), \mathcal{J}(3), \ldots, \mathcal{J}(S)\},$$

where

$$\mathcal{J}(s) = j_{\rm bm}\left(\frac{s-1}{S-1}\alpha\right).$$

Then, for an integer k between 1 and S, we construct k new sequences:

$$\mathcal{J}_k^{(1)} = \left\{\mathcal{J}(1), \mathcal{J}(1+k), \mathcal{J}(1+2k), \ldots, \mathcal{J}\left(1+\left\lfloor\frac{S-1}{k}\right\rfloor k\right)\right\},$$
$$\mathcal{J}_k^{(2)} = \left\{\mathcal{J}(2), \mathcal{J}(2+k), \mathcal{J}(2+2k), \ldots, \mathcal{J}\left(2+\left\lfloor\frac{S-2}{k}\right\rfloor k\right)\right\},$$
$$\ldots\ldots\ldots\ldots\ldots\ldots\ldots\ldots\ldots\ldots\ldots\ldots\ldots\ldots\ldots\ldots\ldots\ldots\ldots\ldots$$
$$\mathcal{J}_k^{(k)} = \left\{\mathcal{J}(k), \mathcal{J}(k+k), \mathcal{J}(k+2k), \ldots, \mathcal{J}\left(k+\left\lfloor\frac{S-k}{k}\right\rfloor k\right)\right\}.$$

Here, $\lfloor\cdot\rfloor$ denotes the floor function. For each sequence $\mathcal{J}_k^{(s)}$, we calculate its "length"

$$L_k^{(s)} = \frac{S-1}{\lfloor\frac{S-s}{k}\rfloor k^2}\sum_{r=1}^{\lfloor\frac{S-s}{k}\rfloor}|\mathcal{J}(s+rk) - \mathcal{J}(s+(r-1)k)|,$$

and then find the average of the lengths

$$L_k = \frac{1}{k}\sum_{s=1}^{k} L_k^{(s)}.$$

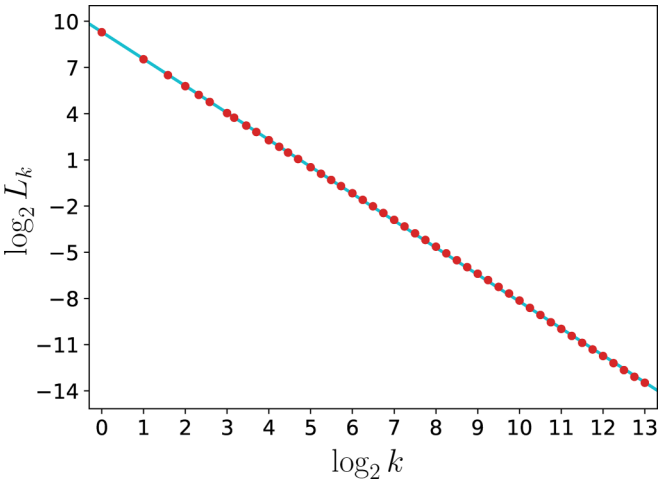

FIG. 3. Dependence of L_k on k. The (red) circles represent the numerically obtained data points. The (turquoise) line is the corresponding line of best fit. See the text for further discussion.

If the curve under investigation is a fractal, then L_k scales with k as

$$L_k \sim 1/k^{D_{\mathrm{H}}},$$

with D_{H} being the Higuchi dimension of the fractal.

Following the above procedure, we calculated L_k for 47 different values of k, ranging between 1 and $8192 = 2^{13}$. Figure 3 shows the results of this calculations on a log-log scale. The (red) circles represent the 47 data points. The (turquoise) line shows the corresponding line of best fit

$$\log_2 L_k = \text{constant} - D_H \log_2 k.$$

The method of least squares gave the following value of the (negative of the) slope of the line

$$D_{\mathrm{H}} = 1.751 \pm 0.0019. \tag{27}$$

This is the sought fractal dimension of the probability current of the backflow-maximizing state. (The intercept is of no importance to our analysis. Merely for reference purposes, it approximately equals 9.309.)

VI. ANALYTICAL APPROXIMATION OF THE BACKFLOW-MAXIMIZING STATE

In this section, we introduce an accurate analytical approximation for the backflow-maximizing state discussed in the previous section. Termed the "guess state," this approximation will be instrumental in exploring the fractal properties of the backflow probability current within the near-optimal regime.

Let us consider the following (guess) state of the particle in a ring

$$\left|\psi_N^{(\mathrm{g})}(t)\right\rangle = C_N\left(|0\rangle - \frac{1}{2}\sum_{m=1}^{N} \mathrm{sinc}(\alpha m^2) e^{-im^2 t}|m\rangle\right), \tag{28}$$

where

$$C_N = \left(1 + \frac{1}{4}\sum_{m=1}^{N} \mathrm{sinc}^2(\alpha m^2)\right)^{-1/2}.$$

The state is normalized to unity, $\langle\psi_N^{(\mathrm{g})}|\psi_N^{(\mathrm{g})}\rangle = 1$. As in the previous section, we take the value of α to be specified by Eq. (23).

For $N = 9999$, which is the value used in the numerical investigations in Sec. V, the guess state provides a very good approximation of the backflow-maximizing state $|\psi_{\mathrm{bm}}\rangle$. The accuracy of the approximation, as quantified by fidelity, exceeds 99%:

$$\left|\left\langle\psi_{9999}^{(\mathrm{g})}\middle|\psi_{\mathrm{bm}}\right\rangle\right|^2 \simeq 0.996328. \tag{29}$$

Let us denote by $j_N^{(\mathrm{g})}(t)$ and $P_N^{(\mathrm{g})}$ the probability current and probability transfer, respectively, associated with the guess state $|\psi_N^{(\mathrm{g})}(t)\rangle$. More precisely,

$$j_N^{(\mathrm{g})}(t) = \left\langle\psi_N^{(\mathrm{g})}(t)\middle|\hat{j}_N\middle|\psi_N^{(\mathrm{g})}(t)\right\rangle$$

and

$$P_N^{(\mathrm{g})} = \int_{-\alpha}^{\alpha} dt\, j_N^{(\mathrm{g})}(t).$$

In terms of numerical calculations, $j_N^{(\mathrm{g})}(t)$ and $P_N^{(\mathrm{g})}$ can be computed from Eqs. (6) and (21), respectively, by taking the expansion coefficient c_m to be those of $|\psi_N^{(\mathrm{g})}(0)\rangle$, i.e., $c_0 = C_N$, and $c_m = -\frac{C_N}{2}\,\mathrm{sinc}(\alpha m^2)$ for $1 \leqslant m \leqslant N$. Thus, we find that the guess state $|\psi_{9999}^{(\mathrm{g})}\rangle$ yields the probability transfer

$$P_{9999}^{(\mathrm{g})} \simeq -0.11131265, \tag{30}$$

which is over 95% of the bound given by Eq. (22). For comparison, in the scenario of a particle on a line, the current analytical approximation record for the backflow probability transfer stands at 70% of the BM bound [30].

The numerical estimates provided by Eqs. (29) and (30) enable us to infer that the family of guess states $|\psi_N^{(\mathrm{g})}\rangle$, as defined in Eq. (28), serves as a good approximation to the backflow-maximizing state for sufficiently large N. Taking this into consideration, we now turn our attention to the limiting state $|\psi_\infty^{(\mathrm{g})}\rangle$, given by Eq. (28) with $N \to \infty$. We argue that the graph representing the corresponding probability current, $j_\infty^{(\mathrm{g})}(t)$, forms a fractal curve with fractal dimension of $\frac{7}{4}$. Our argument relies on the theory outlined in Ref. [55], which can be summarized as follows. Consider a function $f(t)$ defined through the Fourier series

$$f(t) = \sum_l a_l e^{-ilt}. \tag{31}$$

If the coefficients a_l have (pseudo)random phases and the power spectrum scales as

$$|a_l|^2 \sim \frac{1}{l^\beta} \quad (1 < \beta \leqslant 3)$$

as $|l| \to \infty$, then the graphs of $\mathrm{Re}\, f(t)$ and $\mathrm{Im}\, f(t)$ are continuous nondifferentiable curves with fractal dimension

$$D[f] = \frac{5-\beta}{2}.$$

It follows from Eq. (6) that the probability current in question can be expressed as

$$j_\infty^{(\mathrm{g})}(t) = \frac{1}{\pi}\,\mathrm{Re}\{h_0^*(t)h_1(t)\},$$

where

$$h_0(t) = \sum_{m=0}^{\infty} c_m e^{-im^2 t},$$

$$h_1(t) = \sum_{m=0}^{\infty} m c_m e^{-im^2 t},$$

and

$$c_0 = C_\infty,$$
$$c_m = -\frac{C_\infty}{2\alpha}\frac{\sin(\alpha m^2)}{m^2}, \quad (m \geqslant 1).$$

Both series defining h_0 and h_t can be regarded as Fourier series of the form (31) with $l = m^2$, and the $\sin(\alpha m^2)$ term furnishes the pseudorandomness of the Fourier coefficients. Then, the power spectrum corresponding to h_0 scales as $|a_l|^2 \sim |c_m|^2 \frac{dm}{dl} \sim m^{-5} = l^{-5/2}$, yielding $\beta = 5/2$. Hence, the graph of $h_0(t)$ has fractal dimension

$$D[h_0] = \tfrac{5}{4}.$$

In the case of h_1, we have $|a_l|^2 \sim |mc_m|^2 \frac{dm}{dl} \sim m^{-3} = l^{-3/2}$, and $\beta = 3/2$. Hence,

$$D[h_1] = \tfrac{7}{4}.$$

Given that $j_\infty^{(g)}$ is a composite function resulting from the summation of products of two fractal functions, each possessing fractal dimensions of $5/4$ and $7/4$, respectively, it follows that $j_\infty^{(g)}$ is itself a fractal, and its fractal dimension is the larger of the two

$$D\big[j_\infty^{(g)}\big] = \tfrac{7}{4}. \tag{32}$$

As observed, the guess state $|\psi_\infty^{(g)}\rangle$ serves as a good approximation to the numerically exact backflow-maximizing state $|\psi_{\rm bm}\rangle$. Furthermore, the fractal dimension of the probability current linked to the guess state, Eq. (32), aligns closely with the numerical estimate of the fractal dimension characterizing the backflow-maximizing current, Eq. (27). Hence, it is plausible to conjecture that the probability current embodying the true backflow-maximizing state, if it exists, is indeed a fractal with a dimension of $7/4$.

VII. SUMMARY AND DISCUSSION

Motivated to gain deeper insights into the phenomenon of quantum backflow for a particle in a ring, we have taken a careful examination of some properties of the time-dependent probability current through a fixed point on the ring. We showed that when a particle is in a superposition of the $N+1$ lowest-energy eigenstates with nonnegative angular momentum, Eq. (2), the dimensionless probability current can only range between two extreme values, λ_- and λ_+, Eq. (15). λ_-, being the negative extreme value, determines the limit for an instantaneous measurement of the backflow current. The quantum state $|\chi_-\rangle$ corresponding to this extreme value is given by Eqs. (16) and (17).

It is instructive to briefly discuss the regime where $N \gg 1$, wherein the particle state comprises a large number of energy eigenstates. In this regime, the inequalities bounding the dimensionless probability current, given by Eq. (7), simplify to

$$-\frac{\sqrt{\frac{4}{3}}-1}{4\pi}N^2 \leqslant j_N \leqslant \frac{\sqrt{\frac{4}{3}}+1}{4\pi}N^2.$$

For the dimensional probability current, Eq. (5), we have

$$-\frac{\sqrt{\frac{4}{3}}-1}{4\pi}\frac{E_{\max}}{\hbar} \leqslant J_N \leqslant \frac{\sqrt{\frac{4}{3}}+1}{4\pi}\frac{E_{\max}}{\hbar},$$

where $E_{\max} = \frac{\hbar^2 N^2}{2MR^2}$ represents the energy of the particle's highest-energy component. Presented in this form, our result can be compared with a related statement applicable to the scenario of a free particle on a line [12]: $|J| \leqslant \Delta E/\hbar$, where J represents the probability current and ΔE denotes the energy uncertainty of the particle's state. While the two statements are not directly analogous, this comparison offers a complementary perspective.

The second part of this study examines the time dependence of the probability current for particle states that maximize the backflow probability transfer or approach its theoretical bound. First, we perform numerical calculations to determine the backflow-maximizing state (assuming its existence) and compute the fractal dimension of the corresponding probability current versus time function. The obtained numerical value for the fractal dimension, Eq. (27), falls close to $7/4$. Then, we explore an accurate analytical approximation of the backflow-maximizing state, Eq. (28). This analytical state closely aligns with the numerically computed one, exhibiting a fidelity of over 99% and demonstrating backflow probability transfer exceeding 95% of the theoretical bound. (For comparison, in the scenario of a free particle on a line, the state-of-the-art analytical approximation of the backflow-maximizing state captures approximately 70% of the corresponding maximal probability transfer value [30].) The availability of the accurate analytical approximation enables us to analytically evaluate the fractal dimension of the (almost) backflow-maximizing probability current. The analytically predicted value is $7/4$, consistent with the numerical analysis.

The numerical and analytical findings presented in this study strongly suggest that particle-in-a-ring states approaching the probability transfer bound (of approximately 0.116816) exhibit fractal characteristics in the time-dependence of the probability current. This observation is not only interesting in its own right but also offers a signature of quantum backflow. Such a signature could be valuable for future experimental investigations that measure instantaneous current directly (as proposed in Ref. [4]) rather than focusing on integrated probability transfer. Our findings suggest that the instantaneous current will show a highly noisy and irregular time dependence as the system's state approaches backflow-maximizing conditions. This distinctive feature could serve as a guide for exploring the parameter space of the system in search of quantum states that give rise to significant probability backflow.

APPENDIX A: DERIVATION OF EQ. (17)

Real constants $A_\pm$, normalizing

$$|\chi_\pm\rangle = A_\pm \sum_{m=0}^{N} (m + a_\pm)|m\rangle \tag{A1}$$

to unity are found from the requirement that

$$\begin{aligned} 1 &= \langle \chi_\pm | \chi_\pm \rangle \\ &= A_\pm^2 \sum_{m=0}^{N} (m + a_\pm)^2 \\ &= A_\pm^2 \left(\sum_{m=0}^{N} m^2 + 2a_\pm \sum_{m=0}^{N} m + (N+1)a_\pm^2 \right). \end{aligned}$$

Using the identities $\sum_{m=0}^{N} m = \frac{1}{2}N(N+1)$ and $\sum_{m=0}^{N} m^2 = \frac{1}{6}N(N+1)(2N+1) = (N+1)a_\pm^2$, we find

$$A_\pm = [(N+1)(2a_\pm^2 + Na_\pm)]^{-1/2}. \tag{A2}$$

In view of Eq. (14), the above expression for the normalization constants coincides with the one given by Eq. (17).

APPENDIX B: DERIVATION OF EQ. (18)

Starting from Eq. (A1), we rewrite the right-hand side of Eq. (18) as

$$\lambda_+ |\chi_+\rangle\langle\chi_+| + \lambda_- |\chi_-\rangle\langle\chi_-| = \sum_{m,n=0}^{\infty} |m\rangle \mathcal{J}_{mn} \langle n|,$$

where

$$\mathcal{J}_{mn} = \lambda_+ A_+^2 (m + a_+)(n + a_+) + \lambda_- A_-^2 (m + a_-)(n + a_-).$$

Our objective is to establish that $\mathcal{J}_{mn}$ equals $(m+n)/2\pi$ [cf. Eq. (10)]. We have

$$\begin{aligned} \mathcal{J}_{mn} &= (\lambda_+ A_+^2 + \lambda_- A_-^2)mn \\ &\quad + (\lambda_+ A_+^2 a_+ + \lambda_- A_-^2 a_-)(m+n) \\ &\quad + \lambda_+ A_+^2 a_+^2 + \lambda_- A_-^2 a_-^2. \end{aligned} \tag{B1}$$

Using Eqs. (13) and (A2), we get

$$\begin{aligned} \lambda_\pm A_\pm^2 &= \frac{(N+1)(N+2a_\pm)}{4\pi} \frac{1}{(N+1)(2a_\pm^2 + Na_\pm)} \\ &= \frac{1}{4\pi a_\pm}. \end{aligned} \tag{B2}$$

In view of this identity, Eq. (B1) becomes

$$\mathcal{J}_{mn} = \frac{1}{4\pi}\left(\frac{1}{a_+} + \frac{1}{a_-}\right)mn + \frac{1}{2\pi}(m+n) + \frac{a_+ + a_-}{4\pi}.$$

Finally, using fact that $a_+ = -a_-$ [see Eq. (14)], we arrive at the sought result:

$$\mathcal{J}_{mn} = \frac{m+n}{2\pi}.$$

APPENDIX C: DERIVATION OF EQS. (24) AND (25)

Substituting the diagonal representation of the probability current, given by Eq. (19), into Eq. (20), we get

$$P_N = \lambda_+ \int_{-\alpha}^{\alpha} dt\, |\langle \chi_+ | \psi_N(t) \rangle|^2 + \lambda_- \int_{-\alpha}^{\alpha} dt\, |\langle \chi_- | \psi_N(t) \rangle|^2.$$

In view of Eqs. (9) and (A1), we have

$$\langle \chi_\pm | \psi_N(t) \rangle = A_\pm \sum_{m=0}^{N} c_m (m + a_\pm) e^{-im^2 t},$$

so that

$$\begin{aligned} P_N &= \lambda_+ A_+^2 \int_{-\alpha}^{\alpha} dt \left| \sum_{m=0}^{N} c_m (m + a_+) e^{-im^2 t} \right|^2 \\ &\quad + \lambda_- A_-^2 \int_{-\alpha}^{\alpha} dt \left| \sum_{m=0}^{N} c_m (m + a_-) e^{-im^2 t} \right|^2. \end{aligned}$$

Then, taking into account Eq. (B2), we arrive at

$$\begin{aligned} P_N &= \frac{1}{4\pi a_+} \int_{-\alpha}^{\alpha} dt \left| \sum_{m=0}^{N} c_m (m + a_+) e^{-im^2 t} \right|^2 \\ &\quad + \frac{1}{4\pi a_-} \int_{-\alpha}^{\alpha} dt \left| \sum_{m=0}^{N} c_m (m + a_-) e^{-im^2 t} \right|^2 \\ &= P_N^{(+)} + P_N^{(-)}, \end{aligned}$$

which is the representation given by Eqs. (24) and (25).

To better understand the connection between the last representation and the one given by Eq. (21), let us perform the integration over t explicitly and demonstrate that the nonnegative and nonpositive components of the probability transfer indeed add up to the value given by Eq. (21). We have

$$\begin{aligned} P_N^{(\pm)} &= \frac{1}{4\pi a_\pm} \sum_{m,n=0}^{N} c_m^* c_n (m + a_\pm)(n + a_\pm) \int_{-\alpha}^{\alpha} dt\, e^{i(m^2 - n^2)t} \\ &= \frac{\alpha}{2\pi a_\pm} \sum_{m,n=0}^{N} c_m^* c_n (m + a_\pm)(n + a_\pm) \operatorname{sinc}[\alpha(m^2 - n^2)]. \end{aligned}$$

Then,

$$P_N^{(+)} + P_N^{(-)} = \frac{\alpha}{\pi} \sum_{m=0}^{N} \sum_{n=0}^{N} c_m^* c_n S_{mn} \operatorname{sinc}[\alpha(m^2 - n^2)],$$

where

$$S_{mn} = \frac{(m + a_+)(n + a_+)}{2a_+} + \frac{(m + a_-)(n + a_-)}{2a_-}.$$

Finally, using the fact that $a_- = -a_+$ [see Eq. (14)], we obtain

$$S_{mn} = \frac{(m + a_+)(n + a_+)}{2a_+} - \frac{(m - a_+)(n - a_+)}{2a_+} = m + n.$$

This implies that

$$P_N^{(+)} + P_N^{(-)} = \frac{\alpha}{\pi} \sum_{m=0}^{N} \sum_{n=0}^{N} c_m^* c_n (m + n) \operatorname{sinc}[\alpha(m^2 - n^2)].$$

The expression in the right-hand side of this equality coincides with the one in the right-hand side of Eq. (21).

[1] G. R. Allcock, The time of arrival in quantum mechanics III. The measurement ensemble, Ann. Phys. (NY) **53**, 311 (1969).

[2] J. Kijowski, On the time operator in quantum mechanics and the Heisenberg uncertainty relation for energy and time, Rep. Math. Phys. **6**, 361 (1974).

[3] R. F. Werner, Wigner quantisation of arrival time and oscillator phase, J. Phys. A: Math. Gen. **21**, 4565 (1988).

[4] A. J. Bracken and G. F. Melloy, Probability backflow and a new dimensionless quantum number, J. Phys. A: Math. Gen. **27**, 2197 (1994).

[5] S. P. Eveson, C. J. Fewster, and R. Verch, Quantum inequalities in quantum mechanics, Ann. Henri Poincaré **6**, 1 (2005).

[6] M. Penz, G. Grübl, S. Kreidl, and P. Wagner, A new approach to quantum backflow, J. Phys. A: Math. Gen. **39**, 423 (2006).

[7] D. Trillo, T. P. Le, and M. Navascués, Quantum advantages for transportation tasks - projectiles, rockets and quantum backflow, npj Quantum Inf. **9**, 69 (2023).

[8] G. F. Melloy and A. J. Bracken, The velocity of probability transport in quantum mechanics, Ann. Phys. (Berlin, Ger.) **510**, 726 (1998).

[9] M. V. Berry, Quantum backflow, negative kinetic energy, and optical retro-propagation, J. Phys. A: Math. Theor. **43**, 415302 (2010).

[10] H. Bostelmann, D. Cadamuro, and G. Lechner, Quantum backflow and scattering, Phys. Rev. A **96**, 012112 (2017).

[11] J. G. Muga, J. P. Palao, and C. R. Leavens, Arrival time distributions and perfect absorption in classical and quantum mechanics, Phys. Lett. A **253**, 21 (1999).

[12] J. G. Muga and C. R. Leavens, Arrival time in quantum mechanics, Phys. Rep. **338**, 353 (2000).

[13] J. A. Damborenea, I. L. Egusquiza, G. C. Hegerfeldt, and J. G. Muga, Measurement-based approach to quantum arrival times, Phys. Rev. A **66**, 052104 (2002).

[14] J. J. Halliwell, H. Beck, B. K. B. Lee, and S. O'Brien, Quasiprobability for the arrival-time problem with links to backflow and the Leggett-Garg inequalities, Phys. Rev. A **99**, 012124 (2019).

[15] P. Strange, Large quantum probability backflow and the azimuthal angle–angular momentum uncertainty relation for an electron in a constant magnetic field, Eur. J. Phys. **33**, 1147 (2012).

[16] V. D. Paccoia, O. Panella, and P. Roy, Angular momentum quantum backflow in the noncommutative plane, Phys. Rev. A **102**, 062218 (2020).

[17] A. Goussev, Quantum backflow in a ring, Phys. Rev. A **103**, 022217 (2021).

[18] M. Barbier, A. Goussev, and S. C. L. Srivastava, Unbounded quantum backflow in two dimensions, Phys. Rev. A **107**, 032204 (2023).

[19] M. Barbier, Quantum backflow for many-particle systems, Phys. Rev. A **102**, 023334 (2020).

[20] S. V. Mousavi and S. Miret-Artés, Quantum backflow for dissipative two-identical-particle systems, Results Phys. **19**, 103426 (2020).

[21] F. Albarelli, T. Guaita, and M. G. A. Paris, Quantum backflow effect and nonclassicality, Int. J. Quantum Inf. **14**, 1650032 (2016).

[22] S. V. Mousavi and S. Miret-Artés, Dissipative quantum backflow, Eur. Phys. J. Plus **135**, 324 (2020).

[23] S. V. Mousavi and S. Miret-Artés, Erratum to: Dissipative quantum backflow, Eur. Phys. J. Plus **135**, 654 (2020).

[24] G. F. Melloy and A. J. Bracken, Probability backflow for a Dirac particle, Found. Phys. **28**, 505 (1998).

[25] H. Su and J. Chen, Quantum backflow in solutions to the Dirac equation of the spin-1/2 free particle, Mod. Phys. Lett. A **33**, 1850186 (2018).

[26] J. M. Ashfaque, J. Lynch, and P. Strange, Relativistic quantum backflow, Phys. Scr. **94**, 125107 (2019).

[27] Z. Bialynicka-Birula I. Bialynicki-Birula and S. Augustynowicz, Backflow in relativistic wave equations, J. Phys. A: Math. Theor. **55**, 255702 (2022).

[28] L. Di Bari, V. D. Paccoia, O. Panella, and P. Roy, Quantum backflow for a massless Dirac fermion on a ring, Phys. Lett. A **474**, 128831 (2023).

[29] D. Biswas and S. Ghosh, Quantum backflow across a black hole horizon in a toy model approach, Phys. Rev. D **104**, 104061 (2021).

[30] J. M. Yearsley, J. J. Halliwell, R. Hartshorn, and A. Whitby, Analytical examples, measurement models, and classical limit of quantum backflow, Phys. Rev. A **86**, 042116 (2012).

[31] A. J. Bracken and J. B. McGuire, Remarks on quantum probability backflow, arXiv:1608.07644.

[32] A. J. Bracken, Probability flow for a free particle: new quantum effects, Phys. Scr. **96**, 045201 (2021).

[33] S. V. Mousavi and S. Miret-Artés, Different routes to the classical limit of backflow, J. Phys. A: Math. Theor. **55**, 475302 (2022).

[34] J. J. Halliwell, E. Gillman, O. Lennon, M. Patel, and I. Ramirez, Quantum backflow states from eigenstates of the regularized current operator, J. Phys. A: Math. Theor. **46**, 475303 (2013).

[35] I. Chremmos, Design of quantum backflow in the complex plane, J. Phys. A: Math. Theor. **57**, 055301 (2024).

[36] M. Miller, W. C. Yuan, R. Dumke, and T. Paterek, Experiment-friendly formulation of quantum backflow, Quantum **5**, 379 (2021).

[37] M. Barbier and A. Goussev, On the experiment-friendly formulation of quantum backflow, Quantum **5**, 536 (2021).

[38] A. Goussev, Equivalence between quantum backflow and classically forbidden probability flow in a diffraction-in-time problem, Phys. Rev. A **99**, 043626 (2019).

[39] W. van Dijk and F. M. Toyama, Decay of a quasistable quantum system and quantum backflow, Phys. Rev. A **100**, 052101 (2019).

[40] A. Goussev, Probability backflow for correlated quantum states, Phys. Rev. Res. **2**, 033206 (2020).

[41] P. Strange, Quantum backflow for a free-particle hermite wavepacket, Phys. Scr. **99**, 025017 (2024).

[42] J. M. Yearsley and J. J. Halliwell, An introduction to the quantum backflow effect, J. Phys.: Conf. Ser. **442**, 012055 (2013).

[43] A. J. Bracken and G. F. Melloy, Waiting for the quantum bus: The flow of negative probability, Stud. Hist. Philos. Sci. Part B **48**, 13 (2014).

[44] M. Barbier, C. J. Fewster, A. Goussev, G. V. Morozov, and S. C. L. Srivastava, Comment on 'Backflow in relativistic wave equations', J. Phys. A: Math. Theor. **56**, 138003 (2023).

[45] A. J. Bracken and G. F. Melloy, Comment on 'Backflow in relativistic wave equations', J. Phys. A: Math. Theor. **56**, 138002 (2023).

[46] M. Palmero, E. Torrontegui, J. G. Muga, and M. Modugno, Detecting quantum backflow by the density of a Bose-Einstein condensate, Phys. Rev. A **87**, 053618 (2013).

[47] S. Mardonov, M. Palmero, M. Modugno, E. Y. Sherman, and J. G. Muga, Interference of spin-orbit–coupled Bose-Einstein condensates, Europhys. Lett. **106**, 60004 (2014).

[48] Y. Eliezer, T. Zacharias, and A. Bahabad, Observation of optical backflow, Optica **7**, 72 (2020).

[49] A. Daniel, B. Ghosh, B. Gorzkowski, and R. Lapkiewicz, Demonstrating backflow in classical two beams' interference, New J. Phys. **24**, 123011 (2022).

[50] B. Ghosh, A. Daniel, B. Gorzkowski, and R. Lapkiewicz, Azimuthal backflow in light carrying orbital angular momentum, Optica **10**, 1217 (2023).

[51] A. Goussev and J. Joo, Simulating quantum backflow on a quantum computer, Phys. Scr. **99**, 045104 (2024).

[52] See Supplemental Material at http://link.aps.org/supplemental/10.1103/PhysRevA.110.022216 for the expansion coefficients of the backflow-maximizing state.

[53] T. Higuchi, Approach to an irregular time series on the basis of the fractal theory, Physica D **31**, 277 (1988).

[54] L. Liehr and P. Massopust, On the mathematical validity of the Higuchi method, Physica D **402**, 132265 (2020).

[55] M. V. Berry, Quantum fractals in boxes, J. Phys. A: Math. Gen. **29**, 6617 (1996).